Published in final edited form as:

Science. 2017 November 24; 358(6366): 1033–1037. doi:10.1126/science.aai8830.

Structure-property relationships from universal signatures of plasticity in disordered solids

E. D. Cubuk[1,*], **R. J. S. Ivancic**[2,*], **S. S. Schoenholz**[1,2,*], **D. J. Strickland**[3,*], **A. Basu**[2], **Z. S. Davidson**[2], **J. Fontaine**[4], **J. L. Hor**[5], **Y.-R. Huang**[5], **Y. Jiang**[6], **N. C. Keim**[6,7], **K. D. Koshigan**[4], **J. A. Lefever**[3], **T. Liu**[8], **X.-G. Ma**[2,9], **D. J. Magagnosc**[3], **E. Morrow**[10], **C. P. Ortiz**[2], **J. M. Rieser**[2], **A. Shavit**[5], **T. Still**[2], **Y. Xu**[2], **Y. Zhang**[8], **K. N. Nordstrom**[11], **P. E. Arratia**[6], **R. W. Carpick**[6], **D. J. Durian**[2], **Z. Fakhraai**[8], **D. J. Jerolmack**[12], **Daeyeon Lee**[5], **Ju Li**[13], **R. Riggleman**[5], **K. T. Turner**[6], **A. G. Yodh**[2], **D. S. Gianola**[14,†], and **Andrea J. Liu**[2,†]

[1]Google Brain, Mountain View, CA 94043, USA

[2]Department of Physics and Astronomy, University of Pennsylvania, Philadelphia, PA 19104, USA

[3]Department of Materials Science and Engineering, University of Pennsylvania, Philadelphia, PA 19104, USA

[4]Laboratoire de Tribologie et Dynamique des Systémes, École Centrale de Lyon, CNRS UMR 5513, Université de Lyon, 69134 Ecully Cedex, France

[5]Department of Chemical and Biomolecular Engineering, University of Pennsylvania, Philadelphia, PA 19104, USA

[6]Department of Mechanical Engineering and Applied Mechanics, University of Pennsylvania, Philadelphia, PA 19104, USA

[7]Physics Department, California Polytechnic State University, San Luis Obispo, CA 93407, USA

[8]Department of Chemistry, University of Pennsylvania, Philadelphia, PA 19104, USA

[9]Complex Assemblies of Soft Matter, CNRS-Solvay-UPenn UMI 3254, Bristol, PA 19007, USA

[10]Department of Physics, Houghton College, Houghton, NY 14744, USA

[11]Department of Physics, Mount Holyoke College, South Hadley, MA 01075, USA

[12]Department of Earth and Environmental Sciences, University of Pennsylvania, Philadelphia, PA 19104, USA

[†]Corresponding author. ajliu@physics.upenn.edu (A.J.L.); gianola@engr.ucsb.edu (D.S.G.).
[*]These authors contributed equally to this work.

The authors declare that they have no competing financial interests.

SUPPLEMENTARY MATERIALS

www.sciencemag.org/content/358/6366/1033/suppl/DC1

Materials and Methods
Figs. S1 to S12
Tables S1 to S3
Movies S1 and S2
References (46–99)

[13]Department of Nuclear Science and Engineering and Department of Materials Science and Engineering, Massachusetts Institute of Technology, Cambridge, MA 02139, USA

[14]Materials Department, University of California, Santa Barbara, CA 93106, USA

Abstract

When deformed beyond their elastic limits, crystalline solids flow plastically via particle rearrangements localized around structural defects. Disordered solids also flow, but without obvious structural defects. We link structure to plasticity in disordered solids via a microscopic structural quantity, “softness,” designed by machine learning to be maximally predictive of rearrangements. Experimental results and computations enabled us to measure the spatial correlations and strain response of softness, as well as two measures of plasticity: the size of rearrangements and the yield strain. All four quantities maintained remarkable commonality in their values for disordered packings of objects ranging from atoms to grains, spanning seven orders of magnitude in diameter and 13 orders of magnitude in elastic modulus. These commonalities link the spatial correlations and strain response of softness to rearrangement size and yield strain, respectively.

Disordered materials such as metallic glasses have desirable properties such as high strength and stiffness, ultrasmooth surfaces, corrosion resistance, and ultralow mechanical dissipation (1–5). Their widespread use is limited because they tend to fail in a catastrophic, brittle fashion (6–9). Brittle failure likewise hinders applications of amorphous carbon (10), functional nanoparticle films (11, 12), and colloidal packings (13). These complex failure modes also limit our understanding of granular systems and symptoms of failure modes such as avalanches and earthquakes (2, 14–16).

In many cases, the failure process starts with plastic deformation characterized by rearrangements of constituent atoms or particles. Rearrangements can occur at any strain, even when the material response appears nominally elastic, but they do not begin to play a prominent role in relaxing stress until the strain reaches the macroscopically evident yield strain. In crystalline solids, rearrangements at defects such as dislocations typically allow for plastic flow even at strains well above the yield strain, leading to a ductile response. In disordered solids, by contrast, initially localized and homogeneously distributed rearrangements often proliferate rapidly above the yield strain, coalescing to form shear bands (6, 17). This process is considered the culprit behind unpredictable and often catastrophic failure.

Here, we focus on the structural underpinnings of the size of rearrangements at low strains, where rearrangements are localized and homogeneously distributed, and the magnitude of the yield strain. In crystals, most rearrangements occur at dislocations, rendering the task of linking these measures to structure relatively straightforward. For disordered solids, structural fingerprints of rearrangements are subtle. We exploit a recently introduced, machine-learned microscopic structural quantity, “softness,” which has been shown to be strongly predictive of rearrangements in disordered solids (18) and has expanded our conceptual understanding of glassy liquids (19, 20) and aging glasses (21). We link the

spatial correlations of softness to the size of rearrangements, and we link the strain response of softness to the yield strain.

We conducted experiments and simulations on a range of materials including amorphous carbon, silica, metallic glasses, small-molecule and oligomeric glasses, nanoparticle packings, colloidal systems, aqueous foams, and granular packings (22) (see figs. S2 to S4, S6, S7, and S10 to S12). In many of these systems, the interparticle interactions are purely repulsive, whereas in others there is metallic, covalent, or van der Waals bonding. Some of the systems are two-dimensional (2D), but most are 3D. Moreover, the rearrangements have differing origins. In packings of atoms, molecules, and smaller colloids, thermal fluctuations can induce rearrangements even in the absence of any mechanical load. Under applied load, both the incurred stress and the temperature can contribute to rearrangements. In aqueous foams, which are disordered packings of air bubbles, some of the rearrangements are induced by load while others are caused by the coarsening process, in which large bubbles grow at the expense of smaller ones. In larger colloids and granular packings, all of the rearrangements are induced by the applied load. We consider a variety of loading geometries including indentation, uniaxial loading of pillars under extension or tension, and simple shear.

Common rearrangement size in disordered solids

We begin by characterizing the size of rearrangements, which are the precursors to global plasticity. Rearrangements (or the initial rearrangements in an avalanche) have been recognized as being localized in systems such as Lennard-Jones glasses (23), bubble rafts (24), foams (25), and colloidal glasses (26). Frameworks such as shear transformation zone theory start with the assumption that rearrangements are localized (23, 27). Nonetheless, a consistent quantitative measure of their size has been lacking. For systems in which we can obtain the particle positions in real space as a function of time, namely colloidal and granular packings or computational models, it is essential to distinguish rearrangements from other types of displacements without specifying the nature of the rearrangement. To do so, we follow the literature and evaluate the quantity $D^2_{\min}$ between times t and $t + \Delta t$ (23). This quantity captures the mean square deviation of a particle's position from the best-fit affine deformation of its neighborhood,

$$D^2_{\min} = \frac{1}{M_k} \sum_{i}^{M_k} \left[\mathbf{r}_{ik}(t + \Delta t) - \mathbf{J}_k(t) \mathbf{r}_{ik}(t) \right]^2 \quad (1)$$

and therefore measures the nonaffine motion of particle k at time t (23). Here, $\mathbf{r}_{ik}(t)$ is the displacement vector between particles i and k at time t, $\mathbf{J}_k(t)$ is the "best-fit" local deformation gradient tensor about particle k that minimizes $D^2_{\min}(k; t)$, and the summation runs over the M_k particles within a radius R^D_c of particle k.

To measure the spatial extent of rearrangements, we consider the normalized correlation function

$$\left\langle \delta D^2_{\min}(0)\delta D^2_{\min}(r) \right\rangle \equiv \frac{\left\langle D^2_{\min}(0)D^2_{\min}(r)\right\rangle - \left\langle D^2_{\min}\right\rangle^2}{\left\langle \left[D^2_{\min}\right]^2\right\rangle - \left\langle D^2_{\min}\right\rangle^2} \quad (2)$$

Note that the result depends on the time interval Δt used to define $D^2_{\min}$. Many of the systems we study exhibit avalanches near yielding, where an initial localized rearrangement can trigger others, leading to a cascade. To focus on the initial rearrangement, we calculate $D^2_{\min}$ at the value of Δt corresponding to the minimum of the correlation length ξ_r (22) (see fig. S1). It also depends on the size of the neighborhood R^D_c; we find that ξ_r is insensitive to R^D_c as long as it lies somewhere between the first and second peaks of the pair correlation function, $g(r)$ (22) (see fig. S1). Figure 1A demonstrates the exponential decay of $\left\langle \delta D^2_{\min}(0)\delta D^2_{\min}(r)\right\rangle$ with r in units of the particle diameter d two different systems selected from our broader study: a 3D melt of short polymer chains, in which the diameter d corresponds to the size of a monomer, and a 2D bidisperse granular pillar, where d represents the diameter of the larger particles. Indeed, for all of the experimental and computational systems studied, we find that the correlations are reasonably well described by an exponential decay with a correlation length ξ_r (see figs. S2B, S3B, S5B, S8B, and S9B). We therefore characterize the size of rearrangements by ξ_r. Note that this length scale is distinct from that associated with dynamical heterogeneities near the glass transition (28). The first quantity is obtained from $D^2_{\min}$ calculated over a microscopic time scale; the second quantity is measured over a longer time period and is considerably larger because an initial rearrangement of size ξ_r can spread in avalanche fashion (29).

In crystalline systems, rearrangements are concentrated at crystalline defects and therefore reflect spatial correlations associated with the dimensionality and spatial extent of the specific defects. Planar defects such as grain boundaries delineate crystal-crystal interfaces, whereas linear defects such as dislocations can take on complex and spatially extended configurations with a multitude of characters (edge, screw, or mixed). These details can vary enormously from one crystalline system to another and will inevitably affect ξ_r. Furthermore, not all crystalline defects can produce plastic strain (e.g., immobile grain boundaries). We therefore do not expect any commonality in the value of ξ_r for crystalline systems.

Our analysis of disordered solids draws a striking contrast. Overall we have studied 12 different systems. For six of these systems, which span almost the entire range covered by the 12 systems in terms of Young's modulus, particle size, and particle interactions, we have obtained the particle position versus time data needed for the analysis of rearrangement size. Specifically, three of these systems are computational disordered solids, all in 3D [the van Beest, Kramer, and van Santen (BKS) silica model (30), the Kob-Andersen model of a Lennard-Jones glass (31), and oligomer glass pillars (32)] and three are experimental

disordered solids [3D colloidal pillars, 2D granular pillars, and 2D poly(*N*-isopropyl acrylamide) (PNIPAM) colloid glasses]. Figure 2A compiles our results for ξ_r versus particle diameter. The results fall very close to the line of best fit, $\xi_r/d = 1.1 \pm 0.2$, where d is the effective particle diameter (22). In the inset of Fig. 2A, we show the ratio ξ_r/d for the same systems on a log-linear scale; this more unforgiving way of plotting our results shows the adherence to a common value of ξ_r/d.

Linking softness to rearrangements

Mounting evidence has shown that rearrangements across a wide array of disordered materials depend on local structure and energetics (33–37). It has been shown that local yield stress is an excellent predictor of rearrangements in athermal glasses (37). However, calculation of local yield stress requires knowledge of interparticle interactions; this is often difficult to obtain in experimental systems such as colloidal and granular packings, which are naturally polydisperse. Several of us (19, 21) have shown that local structure alone can be used to develop a predictive description of dynamics in glassy liquids (19) and aging glasses (21). Central to the approach is the introduction of "softness," a particle-based quantity that depends only on the local structural environment of the particle. Thus, softness can be determined from any static picture (or snapshot) of the structure along deformation, time, or temperature trajectories. Softness is essentially a weighted integral over the local pair correlation function $g_I(r)$ (20). Using a machine-learning approach akin to linear regression (22), the weighting function is designed to optimize the prediction accuracy for rearrangements (19). In Lennard-Jones glasses (19) and oligomer glasses (38), it has been shown that the energy barrier that must be surmounted for the particle to rearrange decreases linearly with increasing softness. Thus, rearrangements are exponentially more likely to involve particles with high softness. Note that just as not all dislocations contribute to plasticity in crystals, not all high-softness particles participate in rearrangements; like particles surrounding dislocations, soft particles are simply more likely to rearrange than others.

Because high-softness particles are much more likely to rearrange, one would expect the size of a rearrangement to be limited by the spatial extent of high-softness regions. In analogy to the previous discussion of D^2_{min}, we quantify the size of structural heterogeneities by considering the normalized spatial correlation function,

$$\left\langle \delta S(0)\delta S(r) \right\rangle \equiv \frac{\langle S(0)S(r)\rangle - \langle S\rangle^2}{\langle S\rangle^2 - \langle S\rangle^2} \quad (3)$$

As with D^2_{min}, we find that $\langle \delta\Delta S(0)\delta S(r)\rangle$ decays approximately exponentially with the correlation length ξ_s, as shown in Fig. 1B for the short-chain polymer glass and granular pillar. Similar plots for the other four systems studied are shown in figs. S2B, S3B, S5A, S8A, and S9A. Thus, ξ_s is a good measure of the size of high-softness regions that are more likely to rearrange. We find that the emergent correlations of S are nearly universal: Fig. 2B shows that like the rearrangement size ξ_r, the spatial correlation length for softness (the size

of soft regions), ξ_s, falls on a common line $\xi_s/d = 1.1 \pm 0.2$ for all systems studied. Thus, ξ_r and ξ_s are strongly correlated. We now ask whether ξ_s is comparable to the size of rearrangements, ξ_r. In Fig. 2C we show the ratio of the size of rearrangements to the size of soft regions, ξ_r/ξ_s. Indeed, we find $\xi_r/\xi_s = 0.97 \pm 0.07$, with a scatter in ξ_r/ξ_s that is significantly smaller than for ξ_r/d or ξ_s/d, even while ξ_r and ξ_s individually vary by more than seven orders of magnitude. Our multiscale analysis provides compelling evidence that the size of rearrangements, ξ_r, is encoded in the size of correlated soft regions in the system, ξ_s, independent of the nature and even the sign of interactions, the dimensionality of the system, and how the rearrangements were induced.

Common yield strain in disordered solids

We next asked whether commonality of plasticity is observed only in microscopic measures (i.e., rearrangement size and softness correlation length) or whether it is also present in macroscopic measures, such as the strain at the onset of yielding. In crystalline systems, the yield strain is strongly dependent on microstructural details. Only in the limit of ideal strength (the theoretical upper limit) is a constant yield strain expected, as a result of the cooperative crystal shearing mechanism needed in this extreme. In crystalline engineering materials, preexisting defects are plentiful and thus the yield strain depends strongly on processing. A common practice in selection of materials for engineering design is to populate a plot of yield strength versus Young's modulus *E*. Slopes drawn on such an "Ashby chart" give one measure of the yield strain. As a basis for comparison, we examined values for crystalline systems categorized by material class, represented in Fig. 3 as clouds. The yield strength of crystalline metals varies by nearly four orders of magnitude despite a relatively small variation in *E*. Semicrystalline polymers, on the other hand, show a relatively small variation in yield strength yet can exhibit large differences in *E*. Clearly, there is no universality in the onset of yielding in crystalline systems, either within a particular material class or overall.

In contrast, it is known that certain classes of disordered materials share a common value of the yield strain (39–41) despite the heterogeneity of atomic or particle positions within the material. A constant value of the yield strain in shear of 2.7% was empirically shown for a set of metallic glasses on the basis of mechanical tests (39) and was further corroborated by atomistic simulations (40). Experiments on uniaxially loaded colloidal pillars showed a similar yield strain even though the elastic moduli were smaller by as much as five orders of magnitude (41).

Here, we extend the Ashby chart for disordered solids from five orders of magnitude (41) to more than 13 orders of magnitude in elastic modulus. To do this, we have expanded the class of disordered systems to include covalently bonded amorphous solids (amorphous carbon) and several different metallic glasses (see table S1) as well as extremely weakly attracting or purely repulsive systems (colloids, aqueous foams, and granular materials; see tables S2 and S3). We include experimental and computational results for systems subjected to various loading conditions (uniaxial compression/tension, indentation, and shear). Figure 3 shows our collated results for yield strength versus *E*. Strikingly, the data collapse onto a single line on this log-log plot with a linear relationship, corresponding to a universal yield strain of ε_y

= 2.9 ± 0.3%. Note that the data collapse is insensitive to the specific definition of the yield strain, as detailed for each system (22). We also include literature values for metallic glasses (39), glassy polymers (42), and simulations of silica (43), which also collapse on the universal curve. We note that although microscopic information is not available in all systems shown in Fig. 3, four of the systems spanning nearly the full range of E values appear in both Figs. 2 and 3. The implication of this result is that the macroscopic shape change (kinematics) needed for the onset of yield is essentially universal in disordered materials, irrespective of the nature of the interparticle or atomic interactions.

Linking softness to yield strain

To draw a link between the yield strain and microscopic structure as quantified by softness, we draw insight from results for glass-forming liquids by noting an analogy between the yield strain ε_y and the glass transition temperature T_g. They respectively mark the strain and temperature at which rearrangements relax the system on the time scale of measurement. In thermal glassy liquids, the average softness $\langle S \rangle$ is controlled by temperature T; the higher T, the higher $\langle S \rangle$ (19). Moreover, it has been shown that there is a relation between relaxation time and $\langle S \rangle$; the higher $\langle S \rangle$, the shorter the relaxation time (21). The shift in $\langle S \rangle$ with T thus provides a structural measure that tells us about the sensitivity of the relaxation time to temperature.

We suggest that the sensitivity of $\langle S \rangle$ to strain ε provides a way of understanding the common value of the yield strain across systems. We consider a neighborhood around particle k that is larger than the neighborhood required to calculate softness, and apply an affine uniaxial extension at fixed volume (pure shear) of magnitude ε to the neighborhood. We then recalculate softness for particle k. The result averaged over all particles is $\langle S(\varepsilon) \rangle$; we also calculate the standard deviation of the softness distribution in the absence of strain, $\sigma_S = \sqrt{\langle S^2 \rangle - \langle S \rangle^2}$. The quantity $\Delta S(\varepsilon) \equiv [\langle S(\varepsilon) \rangle - \langle S(0) \rangle]/\sigma_S$ measures the change of softness due to applied strain in units of the standard deviation of the softness distribution.

Figure 4 shows that $\Delta S(\varepsilon)$ increases with strain ε, indicating an increased likelihood of rearrangements with strain, as expected. A value of $\Delta S(\varepsilon) = 1$ would correspond to a shift of the average softness equal to the standard deviation of the softness distribution. Note that the shift in average softness is an order of magnitude smaller than the standard deviation for all systems over the range of strains studied. The response of softness to strain is characterized by a smooth function that is quite similar quantitatively for all six systems up to (and even beyond) the onset of macroscopic yielding. The inset of Fig. 4 shows the value of $\Delta S(\varepsilon)$ at the common value of the yield strain ε_y as determined from Fig. 3, demonstrating commonality across length scales. This quantitative similarity of the response of softness to strain for all systems studied provides strong evidence that commonality of yield strain has an underlying structural origin.

Discussion

Figures 2, 3, and 4 provide evidence of universality of spatial correlations in the microscopic dynamics and structure connected to plasticity, as well as universality in the onset of

macroscopic yielding and in the response of microscopic structure to strain in disordered solids. These quantitative commonalities transcend the details of constituent size and interactions.

The observed universality lends quantitative credence to the use of model disordered solids as analogs of atomic glasses—for instance, in sheared bubble rafts (24) and colloidal solids (26). Commonalities in the statistics of slip intermittency just above yield among various disordered solids (44, 45) suggest additional universality near yield. One corollary of commonality of yield strain is that one cannot easily increase the strain at the onset of yielding of a disordered solid. A more promising route to increasing the toughness of disordered solids may be to manipulate the evolution of rearrangements above the yield strain, thereby increasing the window of plastic flow between the yield strain and failure. The success of the softness framework in explaining two properties of plasticity near yield suggests that it may also provide a fruitful approach for studying shear band formation in systems beyond yield.

The universal behaviors that we observe are all the more striking because there is no sign of universality in the microscopic packing structure itself. For each system, the definition of softness is different. Universality only becomes apparent once the softness of the constituent particles is considered, where we see emergent commonality in the properties of softness.

In crystals, on the other hand, there is universality in the microscopic structure, in the sense that there is a universal definition of a dislocation independent of constituent size, interactions, or crystal structure. However, the spatial correlations of dislocations vary enormously from one crystalline system to another—a direct consequence of the extended nature of these linear defects. As a result, the emergent properties of crystalline defects are not universal. There is no commonality in the spatial correlations of dislocations, so we expect no commonality in the spatial size of rearrangement events. Likewise, there is no commonality in the yield strain among material classes (Fig. 3). Indeed, most efforts in the modeling of crystal plasticity focus on incorporating specific features of the material under study (e.g., dislocation density and character of dislocations) and the prevailing notion is that no unifying theory is tractable.

The essential differences between plasticity in crystals and plasticity in disordered materials can be summarized as follows. In crystals, there is universality in the definition of the microscopic structural features correlated with rearrangements, but in disordered solids there is not. On the other hand, in disordered solids there is emergent universality in the properties of those features, but in crystals there is not. The origin of this universality is not yet understood. Our results, however, point to the possibility of a unifying framework and a vast simplification of our understanding of plasticity in disordered solids, which paradoxically may not be possible for crystals.

Supplementary Material

Refer to Web version on PubMed Central for supplementary material.

Acknowledgments

This research was primarily supported by NSF through the University of Pennsylvania Materials Research Science and Engineering Center (MRSEC) (DMR-1720530), including its Rheology, Optical and Electron Microscopy Shared Experimental Facilities. We thank the Penn Nanoscale Characterization Facility and the Laboratory for Research on the Structure of Matter (LRSM) Computational Facility. Partial support is acknowledged from NSF grants DMR-1107642 (R.W.C.), DMR-1305199 (D.J.D.), DMR-160738 (A.G.Y.), DMREF-1628407 (Z.F.), CMMI-1724519 (D.S.G.), and INSPIRE/EAR-134428 (D.J.J.); the LRSM Research Experience for Undergraduates program (E.M.); Simons Foundation grant 327939 (A.J.L.); NASA grant NNX08O0G (A.G.Y.); and Agence Nationale de la Recherche grant ANR0110NS09-01 through the Materials World Network program. N.C.K. and P.E.A. acknowledge the donors of the American Chemical Society Petroleum Research Fund (ACS-PRF-53948-ND9) for partial support. Z.F. acknowledges P. J. Walsh (Penn Chemistry) and students E. Salami-Ranjbaran and K. Cheng for tris(naphthyl)benzene (TNB) synthesis.

REFERENCES AND NOTES

1. Trexler MM, Thadhani NN. Prog Mater Sci. 2010; 55:759–839.
2. Jaeger HM, Nagel SR, Behringer RP. Rev Mod Phys. 1996; 68:1259–1273.
3. Bansal NP, , Doremus RH. Handbook of Glass Properties Academic Press; 1986
4. Parmenter KE, Milstein F. J Non-Cryst Solids. 1998; 223:179–189.
5. Nielson LE, , Landel RF. Mechanical Properties of Polymers and Composites Vol. 2. Marcel Dekker; 1981
6. Schuh CA, Hufnagel TC, Ramamurty U. Acta Mater. 2007; 55:4067–4109.
7. Chen M. Annu Rev Mater Res. 2008; 38:445–469.
8. Barthelat F, Rabiei R. J Mech Phys Solids. 2011; 59:829–840.
9. Ritchie RO. Nat Mater. 2011; 10:817–822. [PubMed: 22020005]
10. Robertson J. Mater Sci Eng Rep. 2002; 37:129–281.
11. Herrmann J, et al. Appl Phys Lett. 2007; 91:183105.
12. Zhang L, et al. ACS Nano. 2013; 7:8043–8050. [PubMed: 23971916]
13. Hiemenz PC. Principles of Colloid and Surface Chemistry 2. Marcel Dekker; 1986
14. Nedderman RM. Statics and Kinematics of Granular Materials Cambridge Univ Press; 1992
15. Gidaspow D. Multiphase Flow and Fluidization: Continuum and Kinetic Theory Descriptions Academic Press; 1994
16. Herrmann HJ, , Hovi JP, , Luding S. Physics of Dry Granular Media Kluwer Academic; 1998
17. Greer A, Cheng Y, Ma E. Mater Sci Eng Rep. 2013; 74:71–132.
18. Cubuk ED, et al. Phys Rev Lett. 2015; 114:108001. [PubMed: 25815967]
19. Schoenholz SS, Cubuk ED, Sussman DM, Kaxiras E, Liu AJ. Nat Phys. 2016; 12:469–471.
20. Cubuk ED, Schoenholz SS, Kaxiras E, Liu AJ. J Phys Chem B. 2016; 120:6139–6146. [PubMed: 27092716]
21. Schoenholz SS, Cubuk ED, Kaxiras E, Liu AJ. Proc Natl Acad Sci USA. 2017; 114:263–267. [PubMed: 28028217]
22. See supplementary materials.
23. Falk ML, Langer JS. Phys Rev E. 1998; 57:7192–7205.
24. Argon A, Kuo H. Mater Sci Eng. 1979; 39:101–109.
25. Durian DJ, Weitz DA, Pine DJ. Science. 1991; 252:686–688. [PubMed: 17746666]
26. Schall P, Weitz DA, Spaepen F. Science. 2007; 318:1895–1899. [PubMed: 18096800]
27. Falk ML, Langer JS. Annu Rev Condens Matter Phys. 2011; 2:353–373.
28. Berthier L, , Biroli G, , Bouchaud JP, , Cipelletti L, , van Saarloos W. Dynamical Heterogeneities in Glasses, Colloids, and Granular Media Oxford Univ Press; 2011
29. Candelier R, et al. Phys Rev Lett. 2010; 105:135702. [PubMed: 21230788]
30. van Beest BWH, Kramer GJ, van Santen RA. Phys Rev Lett. 1990; 64:1955–1958. [PubMed: 10041537]
31. Kob W, Andersen HC. Phys Rev Lett. 1994; 73:1376–1379. [PubMed: 10056777]

32. Shavit A, Riggleman RA. Phys Chem Chem Phys. 2014; 16:10301–10309. [PubMed: 24676009]
33. Brito C, Wyart M. J Stat Mech. 2007; 2007:L08003.
34. Ashton DJ, Garrahan JP. Eur Phys J E. 2009; 30:303–307. [PubMed: 19859750]
35. Rottler J, Schoenholz SS, Liu AJ. Phys Rev E. 2014; 89:042304.
36. Schoenholz SS, Liu AJ, Riggleman R, Rottler J. Phys Rev X. 2014; 4:031014.
37. Patinet S, Vandembroucq D, Falk ML. Phys Rev Lett. 2016; 117:045501. [PubMed: 27494480]
38. Sussman DM, Schoenholz SS, Cubuk ED, Liu AJ. Proc Natl Acad Sci USA. 2017; 114:10601–10605. [PubMed: 28928147]
39. Johnson WL, Samwer K. Phys Rev Lett. 2005; 95:195501. [PubMed: 16383993]
40. Cheng YQ, Cao AJ, Sheng HW, Ma E. Acta Mater. 2008; 56:5263–5275.
41. Strickland DJ, Huang YR, Lee D, Gianola DS. Proc Natl Acad Sci USA. 2014; 111:18167–18172. [PubMed: 25489098]
42. Kozey VV, Kumar S. J Mater Res. 1994; 9:2717–2726.
43. Tang C, Da'vila LP. J Appl Phys. 2015; 118:094302.
44. Uhl JT, et al. Sci Rep. 2015; 5:16493. [PubMed: 26572103]
45. Denisov DV, Lörincz KA, Uhl JT, Dahmen KA, Schall P. Nat Commun. 2016; 7:10641. [PubMed: 26883071]

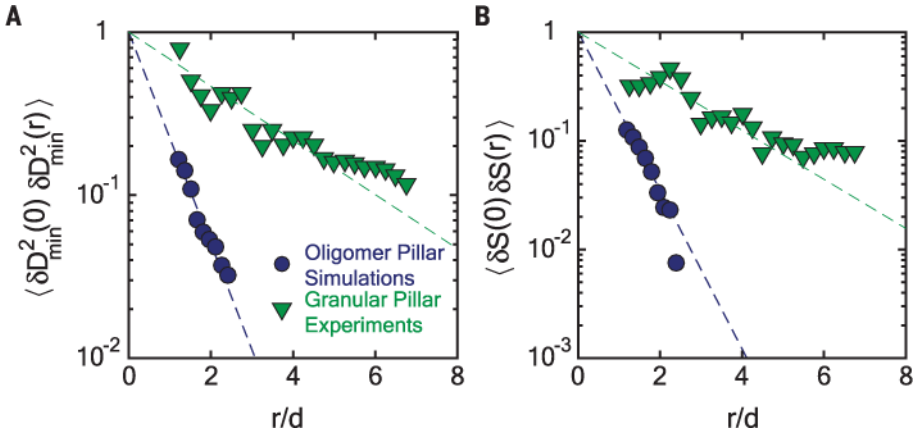

Fig. 1. Spatial correlations in D^2_{min} and softness fields

(**A** and **B**) Spatial correlations in the D^2_{min} field (A) and softness field (B) for two very different systems: a 3D short-chained polymer pillar studied by molecular dynamics simulation (circles) and a 2D bi-dispersed granular pillar studied experimentally (triangles). Here, d is the diameter of a single monomer for the polymer pillar and of a large particle for the granular pillar, and r is the radial distance. The dashed lines are fits to $\exp(-r/\xi_r)$ in (A) and to $\exp(-r/\xi_s)$ in (B), defining the size of rearrangements, ξ_r, and of soft regions, ξ_s. Similar exponential decays hold for all other systems studied (22).

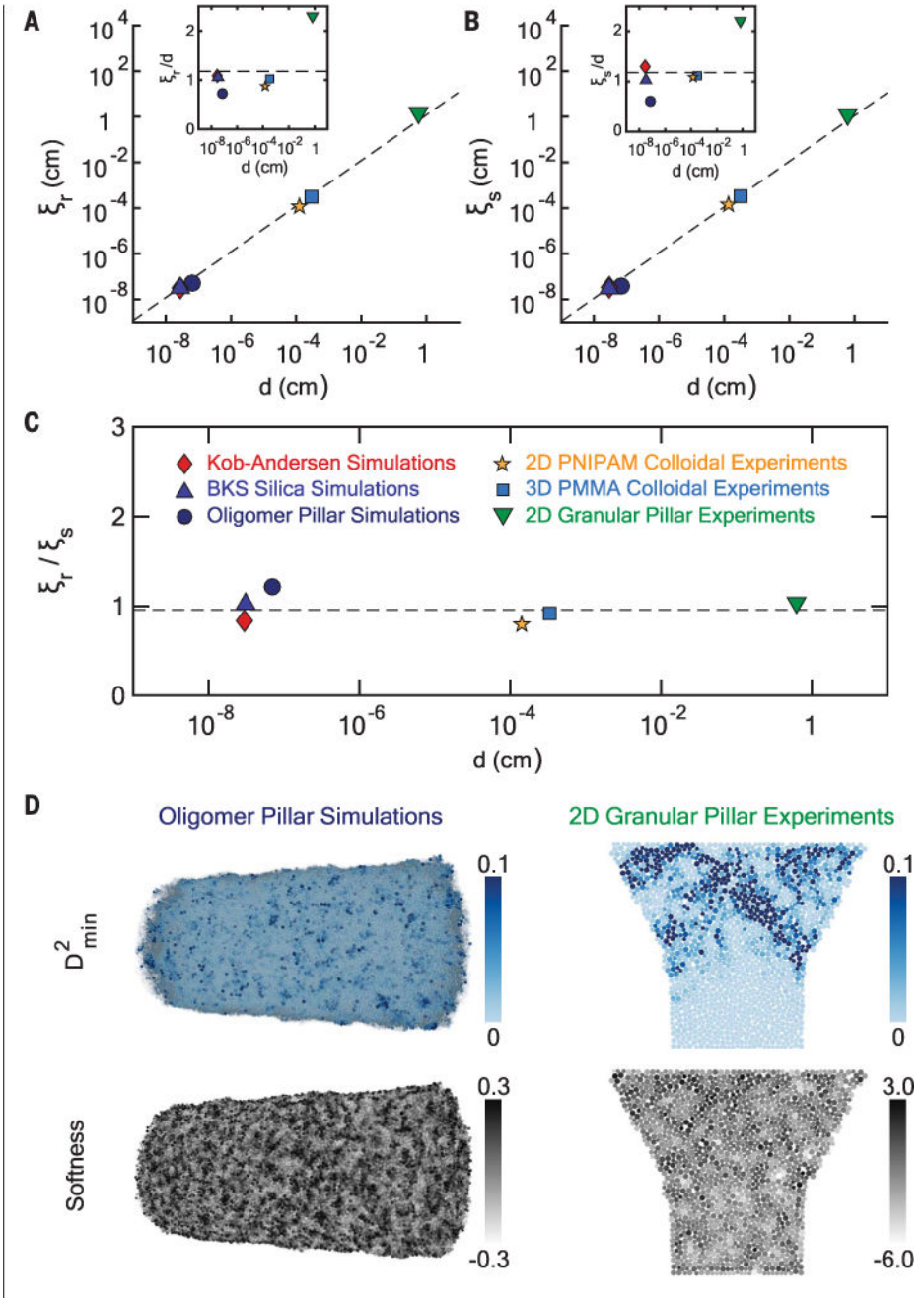

Fig. 2. Microscopic analysis of dynamics and structure

Emergent properties of the D^2_{min} and softness fields for six different materials are shown, as indicated within (C). (**A** and **B**) The correlation lengths of D^2_{min} (A) and softness (B), ξ_r and ξ_s respectively, are plotted against particle diameter d for each material on a log-log scale. The dashed lines in (A) and (B) represent the proportionality relations $\xi_r/d = 1.1 \pm 0.2$ and $\xi_s/d = 1.1 \pm 0.2$, respectively. The insets show ξ_r/d and ξ_s/d, respectively, versus d on a log-linear scale. (**C**) The ratio ξ_r/ξ_s is plotted against d for each material on a log-linear scale.

The average of this ratio is $\xi_r/\xi_s = 0.97 \pm 0.07$ (dashed line). (**D**) Snapshots of the D^2_{min} and softness fields for the oligomer pillar simulation and the granular pillar experiment.

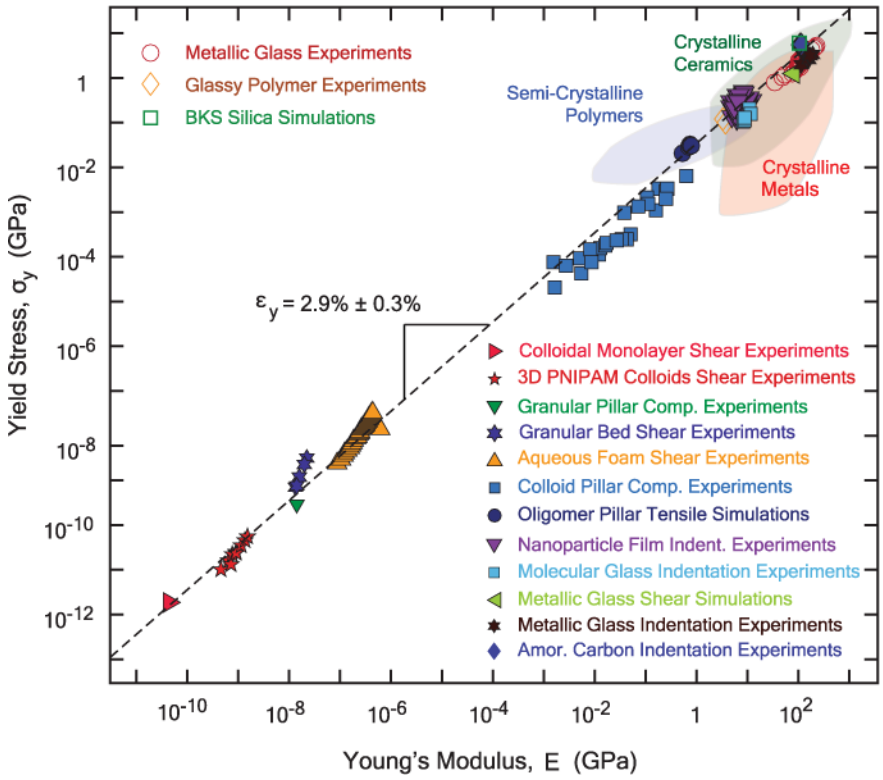

Fig. 3. Macroscopic mechanical response

An Ashby chart shows yield stress σ_y versus Young's modulus E for a variety of experimental and simulated disordered systems. We also include literature values for metallic glass experiments (39), glassy polymer experiments (42), and BKS silica simulations (43). The data collapse onto a single curve, implying a universal yield strain of $\varepsilon_y = 2.9 \pm 0.3\%$ (dashed line). In contrast, crystalline metals (red cloud) show a large variation in strength with little change in E, and semicrystalline polymers (blue cloud) show a wide variation in E with little change in strength. Previously reported crystalline material clouds were generated using Materials Property CES Selector software by Granta Design.

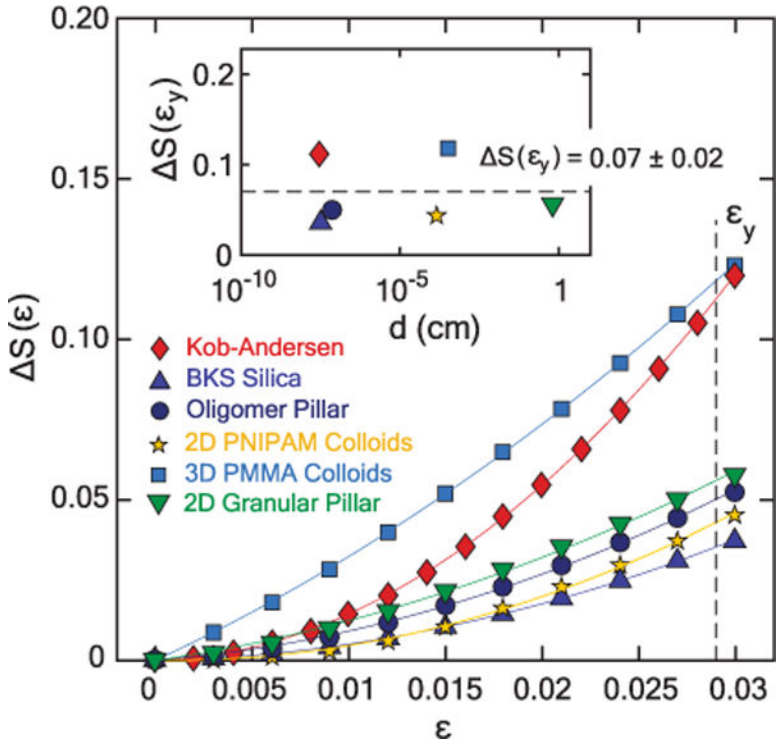

Fig. 4. Response of softness to affine strain

The response of the mean softness to an affine uniaxial extension, ε, for six different materials is quantified using $\Delta S(\varepsilon) = [\langle S(\varepsilon)\rangle - \langle S(0)\rangle]/\sigma_S$, where $\langle S(\varepsilon)\rangle$ the mean softness at a strain of ε and σ_S is the standard deviation of softness at a strain of $\varepsilon = 0$. These data were obtained by applying a uniaxial extension of magnitude ε to the neighborhood about each particle larger than the one used to calculate softness in each material. The softness field for the strained material was calculated using the original hyperplane and then averaged. The dashed line denotes the universal value of yield strain for disordered materials, ε_y. The inset shows values of $\Delta S(\varepsilon_y)$ versus particle diameter d for all six systems. These values are all similar, suggesting that the universality of the yield strain of disordered materials reflects a common response of softness to strain.